BIOCHEMISTRY
including biophysical chemistry & molecular biology

Article

pubs.acs.org/biochemistry

Molecular Clues about the Dystrophin–Neuronal Nitric Oxide Synthase Interaction: A Theoretical Approach

Emmanuel Giudice,[†,‡] Anne-Elisabeth Molza,[†,‡] Yoann Laurin,[†,‡] Aurélie Nicolas,[†,‡] Elisabeth Le Rumeur,[†,‡] and Olivier Delalande*[,†,‡]

[†]Université de Rennes1, 35700 Rennes, France

[‡]UMR CNRS 6290, Institut de Génétique et de Développement de Rennes (IGDR), 35043 Rennes, France

Supporting Information

ABSTRACT: Dystrophin is a large skeletal muscle protein located at the internal face of the plasma membrane and interacting with membrane phospholipids and a number of cytosolic proteins. Binding of neuronal nitric oxide synthase (nNOS) to dystrophin appears to be crucial for exercise-induced increases in blood supply in muscle cells. By contrast, utrophin, the developmental homologous protein of dystrophin, does not display nNOS interaction. Recent *in vitro* and *in vivo* experiments showed that the dystrophin region involved in nNOS binding is located in spectrin-like repeats R16 and R17 of its filamentous central domain. Using homology modeling and atomistic molecular dynamics simulation, we compared the structural organization and surface potentials of dystrophin, utrophin, and chimeric fragments, thus revisiting the dystrophin–nNOS binding region. Our simulation results are in good agreement with experimental data. They provide a three-dimensional representation of the repeats and give insight into the molecular organization of the regions involved in dystrophin–nNOS interaction. This study also further elucidates the physical properties crucial for this interaction, particularly the presence of a large hydrophobic patch. These results will be helpful to improving our understanding of the phenotypic features of patients bearing mutations in the nNOS-binding region of dystrophin.

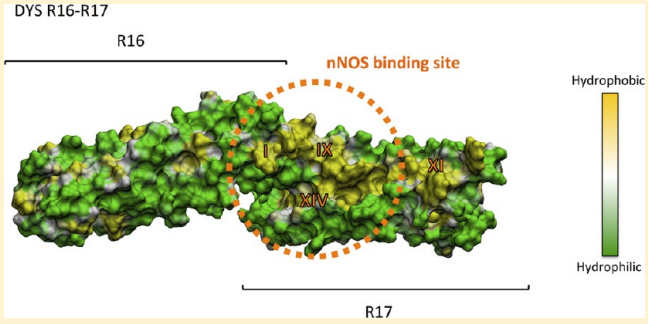

Dystrophin is a large skeletal muscle protein[1] at the internal face of the plasma membrane. Its complete loss due to mutations of the *DMD* gene leads to the severe disease Duchenne muscular dystrophy (DMD), while the expression of an internally deleted dystrophin results in mild to severe Becker muscular dystrophy (BMD).[2] Dystrophin consists of four major domains.[3] The central rod domain is composed of 24 spectrin-like repeats folded in triple-helical coiled-coil domains[4,5] and was long thought to play only a mechanical role in muscle cells. However, recent studies have shown that this domain contributes to the scaffolding activity of the protein by interacting with membrane phospholipids and a number of cytosolic proteins such as filamentous actin, microtubules, and neuronal nitric oxide synthase (nNOS).[3] Among these interactions, that of dystrophin with nNOS appears to be crucial for exercise-induced increases in blood supply in muscle cells. Through the regulation of vasodilatation, nNOS modulates muscular blood flow to ensure the metabolic needs of contracting muscles. Thus, muscles of DMD patients lacking dystrophin are more susceptible to ischemia during exercise.[6] In the muscles expressing internally deleted dystrophin in BMD patients, the mislocalization of nNOS is correlated with an increase in disease severity, likely through alteration of blood flow regulation.[7] Although nNOS was initially thought to interact indirectly with the C-terminus of dystrophin via syntrophin, Lai and co-workers have demonstrated that repeats 16 and 17 of the dystrophin central rod domain (DYS R16 and R17, respectively) are essential for maintaining nNOS at the sarcolemma.[8] The strategy for their work originated in their observation that the homologous protein utrophin does not bind nNOS even though a strong structural similarity exists between the coiled-coil spectrin-like repeats of both dystrophin and utrophin. They initially used a human dystrophin DYS R16–R17 construct and compared it in cellular systems to the homologous repeats 15 and 16 of mouse utrophin (UTR R15 and R16, respectively) and that in a transgenic mouse model. They then tried subtle substitutions of mouse utrophin and human dystrophin short sequences.[9] Using chimeric dystrophin–utrophin constructs (with dystrophin short sequences replaced by their homologous utrophin sequences), the group identified the motif involved in the interaction as a microdomain localized in the N-terminal part of helix A of repeat 17. However, this domain alone is not enough for nNOS to bind to dystrophin, as helices B and C of R16 and R17 are also required to ensure *in vivo* nNOS membrane localization.

Received: February 20, 2013
Revised: September 9, 2013
Published: September 24, 2013

   dx.doi.org/10.1021/bi400794p | *Biochemistry* 2013, 52, 7777–7784

We present here a study based on homology modeling and molecular simulation that provides three-dimensional (3D) structural insight into the molecular clues about the dystrophin−nNOS interaction. We define the essential dystrophin residues for nNOS binding and suggest the nature of their likely contributions.

MATERIALS AND METHODS

Homology Models. For comparison with the work of Lai and co-workers,[8,9] we used four different molecules identical to their constructs: (i) the human DYS R16−R17 dystrophin tandem repeat, (ii) the mouse utrophin UTR R15−R16 repeats, homologous to the dystrophin R16−R17 repeats, (iii) a chimera made of human dystrophin R16 and mouse utrophin R16 (DYS R16−UTR R16), and (iv) another chimera made of mouse utrophin R15 and human dystrophin R17 (UTR R15−DYS R17). As in our previous work,[13] the homology models were all obtained with the I-TASSER web server,[10−12] using an updated template library that included the newly published DYS R1 and UTR R1 structures.[14]

Molecular Dynamics Protocol. To simulate our systems of tandem repeats, water, and ions, we used NAMD version 2.7b2[15] and the CHARMM27 force field.[16,17] The initial models of the dystrophin tandem repeats were oriented along the *z*-axis and then solvated in rectangular water boxes generated using the Solvate plugin of VMD.[18] We thus ensured that there was a 30 Å thick layer of TIP3P water in the *x* and *y* directions and a 15 Å thick layer in the *z* direction. Subsequently, the VMD plug-in Autoionize was used to randomly place ions to neutralize the system while maintaining a NaCl concentration of 150 mM. To adjust the position of the solvent (water and ions) around the molecule, each system was energy-minimized for 10000 steps using the conjugate gradient method while restraining the solute atoms with a 25 kcal mol^{-1} $Å^{-2}$ harmonic restraint. The entire system (solvent and solute) was then subjected to another 10000 steps of energy minimization to relieve any major stresses, followed by a slow heating to 310 K at a constant volume over a period of 50 ps. The production phase was performed for 101 ns under periodic boundary conditions with a 2 fs time step using the SHAKE algorithm. van der Waals interactions were computed using a cutoff distance of 12 Å with a switching function starting at 10 Å, while long-range electrostatic forces were calculated using the particle mesh Ewald method with a grid density of 1 $Å^{-3}$. To further reduce the cost of computing full electrostatics, a multiple-time-step procedure was employed to calculate long-range electrostatics every 4 fs. Berendsen baths were used to maintain the system temperature and pressure at 310 K and 1 atm, respectively.

Trajectory Analysis. The postprocessing analysis of the MD trajectories was performed with VMD[18] and ptraj using the last 96 ns of simulation (the first 5 ns being considered part of the relaxation time of the system). To extract representative structures, the coordinate frames from the trajectory were clustered with the K-Means algorithm, using the pairwise rmsd between frames as a metric to compare the Cα atoms of the protein. After testing various numbers of clusters (two to six), we compared the resulting Davies−Bouldin index (BDI), the pseudo-F statistic (pSF), and the SSR/SST ratio (where SSR is the sum of square regression from each cluster and SST is the total sum of squares) and chose to split the trajectory into two clusters.[19] Electrostatic potentials were computed with APBS[20] using the CHARMM force field and sodium and chloride ion concentrations of 50 mM. Molecular hydrophobicity potentials (MHPs) were computed by the Platinum server,[21] using the Ghose force field parameters. Secondary structure assessments were performed with Stride,[22] and the residues belonging to an α-helix for <80% of the time were used to define the A−B and B−C loops that delimit the helical regions (HA, HB, HCA, HB, and HC). The bending of the helices was analyzed and plotted with Bendix.[23]

RESULTS

The aim of this study is to highlight the dystrophin−nNOS binding site using molecular modeling and simulations performed on constructs known to have different nNOS binding properties. We used four of these: (i) the DYS R16−R17 tandem repeat involved in the interaction with nNOS, (ii) the UTR R15 and R16 repeats (UTR R15−R16), homologous to the DYS R16 and R17 repeats but unable to bind to nNOS, (iii) a chimera made of DYS R16 and UTR R16 (DYS R16−UTR R16) also unable to bind nNOS, and (iv) another chimera made of UTR R15 and DYS R17 (UTR R15−DYS

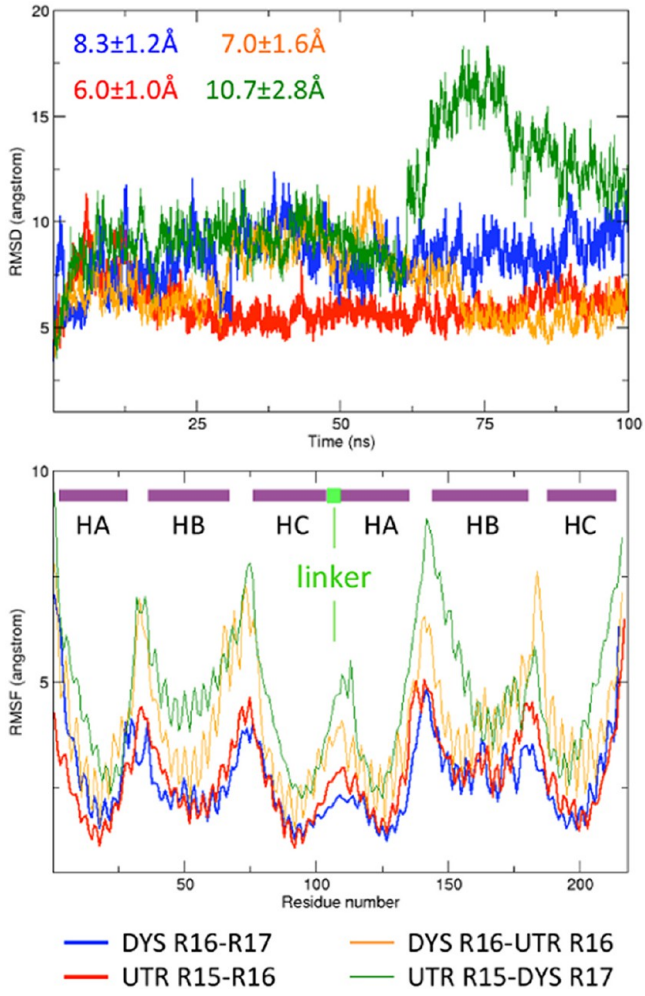

Figure 1. Plots of the Cα root-mean-square deviations (rmsds) and fluctuations (rmsfs) for the four simulated constructs. Both charts indicate that in our MD simulations native tandem repeats UTR R15−R16 (red) and DYS R16−R17 (blue) are more stable than chimeric fragments (orange and green). Global rmsds of bending fragments exhibit higher mean values, while chimeric fragments present higher standard deviations related to a higher rmsf.

dx.doi.org/10.1021/bi400794p | *Biochemistry* 2013, 52, 7777−7784

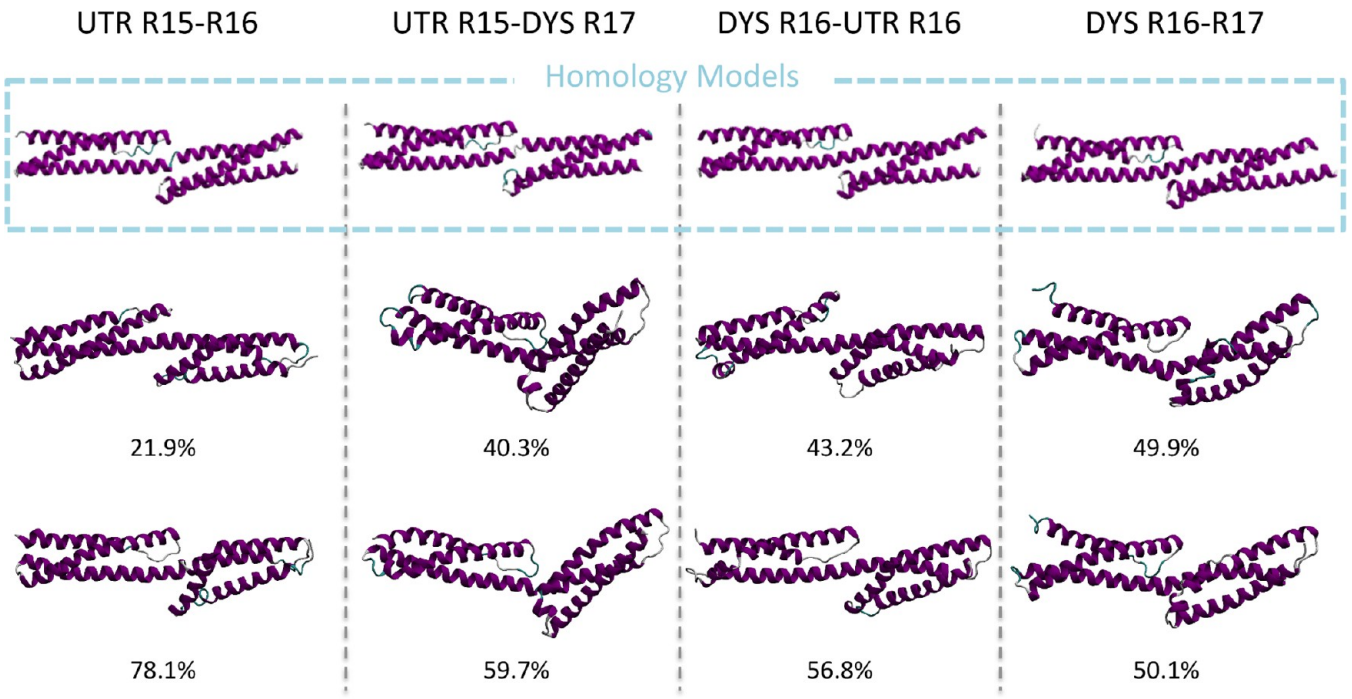

Figure 2. Initial structures (I-TASSER homology model) and the most representative conformers of each MD trajectory computed for UTR R15−R16, UTR R15−DYS R17, DYS R16−UTR R16, and DYS R16−R17. For the representative conformers, the size of the corresponding clusters is indicated as a percentage of the whole trajectory.

R17) partially recruiting nNOS to the membrane. This helped us to understand the structural and physical properties of dystrophin as it pertains to dystrophin−nNOS interaction.

Structural Stability of Coiled-Coil Tandem Repeats. The I-TASSER *C* scores (0.52−0.76 depending on the models) and the ProCheck results (see the homology modeling section in the Supporting Information) indicate that the structural models are high quality. The four models have 3D coiled-coil structures that are maintained along the 100 ns trajectories (Figure 1). However, the two chimeras mixing UTR and DYS repeats seemed slightly less stable, as shown by the larger amplitude of their root-mean-square deviations and fluctuations (rmsds and rmsfs, respectively) (Figure SM1 of the Supporting Information). The rmsd measured for individualized repeats showed that the main variations of the global rmsd are induced by changes in the relative positioning of the two consecutive repeats. The hydrophobic residues composing the heptad pattern that maintain the triple-helical coiled-coil structure of the repeats are easily retrieved at the minimal peaks of the rmsf plots (Figure 1). The linker regions of chimeric fragments also appear to be less stable in comparison to the native ones. The major changes observed in the global structure involve the surrounding residues of the linker regions, where the B helices tend to move away from each other in the two chimeras mixing UTR and DYS repeats (Figures 1 and 2). Therefore, the relative positioning of α-helices between consecutive repeats appears to be highly dependent on the structural stability of the linker region. It is important to note that the two models that include DYS R17 (DYS R16−17 and UTR R15−DYS R17) kink between their successive repeats at the linker region, while UTR R15−R16 and DYS R16−UTR R16 tandem repeats remain straight.

Molecular Surface Potentials. To assess the relative importance of electrostatics and hydrophobicity, the two main driving forces for protein−protein interaction, we calculated the molecular surface properties of the representative conformations extracted through the clustering analysis of the MD trajectories of each protein construct. As we previously observed,[13] we identified a substantial heterogeneity of both electrostatic (Figure 3) and hydrophobicity potentials (Figure 4) between dystrophin repeats R16 and R17. It appears that this is also the case for utrophin repeats R15 and R16, as expected considering their differing pHi.[24] For the most part, each isolated repeat present in the chimeric fragments conserves the global surface properties observed in native dystrophin and utrophin repeats, and only slight changes were found in the vicinity of the linker region (Figures 3A and 4A).

Although they are not identically distributed, similar electrostatic profiles were observed for the homologous DYS R16 and UTR R15, with the exception of two patches located on the A−B and B−C loops. By contrast, the electrostatic surface potentials of DYS R17 and UTR R16 differ markedly, with a globally neutral potential in the region comprising residues Arg115−Arg167 of DYS R17, and a globally negative potential in the UTR R16 homologous region comprising residues Gln115−Ile168 (Figure 3A). At the 3D molecular level, this results in the formation of a strong electronegative field surrounding the middle of the UTR R16 coiled coil (Figure 3B and Figure SM2 of the Supporting Information).

Differences were also found in the molecular hydrophobicity potential profiles of these repeats (Figure 4A). They arise from the 3D distribution of the hydrophobic residues, in particular, Phe35 and Phe39 in DYS R16 and those located between Tyr118 and Phe123 and between Tyr148 and Leu152 in DYS R17. Together, these residues form a large hydrophobic patch positioned along the interface of helices A and B. The three hydrophobic residues Trp113, Phe116, and Ile187 also contribute to this patch, extending it to the interface of helices A and C of DYS R17. This hydrophobic patch is replaced by a hydrophilic region in the fragments missing DYS R17, i.e., UTR

dx.doi.org/10.1021/bi400794p | *Biochemistry* 2013, 52, 7777−7784

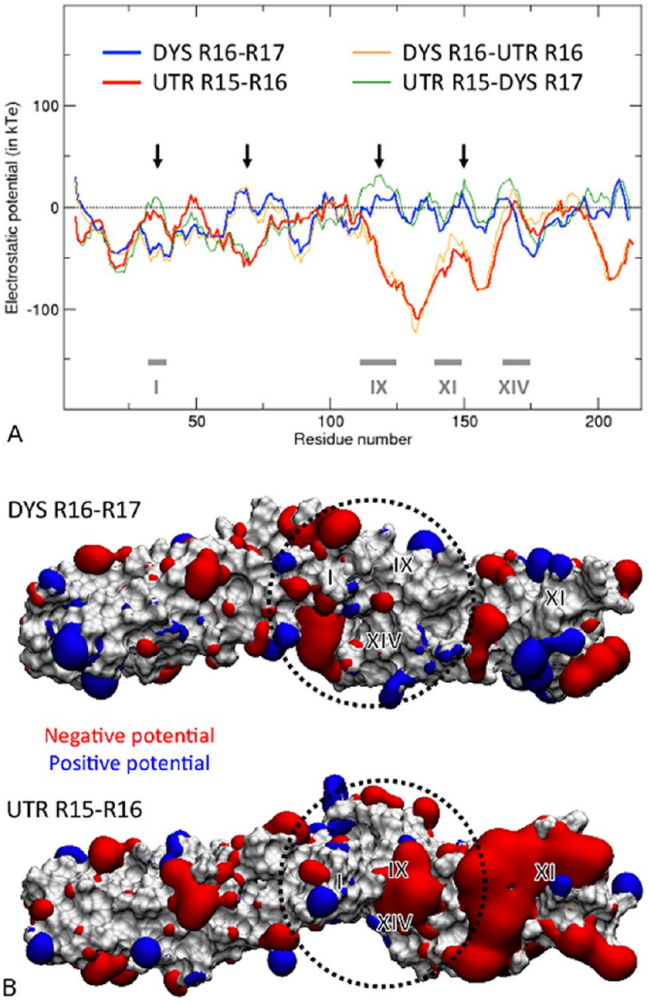

Figure 3. (A) Electrostatics averaged over the major conformational states of the tandem repeats. Arrows indicate the regions showing the major differences between the UTR R15−R16 and DYS R16−R17 fragments. Along the primary sequence, we indicate the position of microdomains I, IX, XI, and XIV that induce the largest modifications of nNOS membrane localization, as reported by Lai and co-workers. (B) 3D isovolume representation of the electrostatic surface potentials of the major conformations of both dystrophin and utrophin tandem repeats as calculated with APBS [50 *kTe* (blue) and −50 *kTe* (red)]. Circles with dashed black lines indicate the region that differentiates between fragments interacting with nNOS and those that do not.

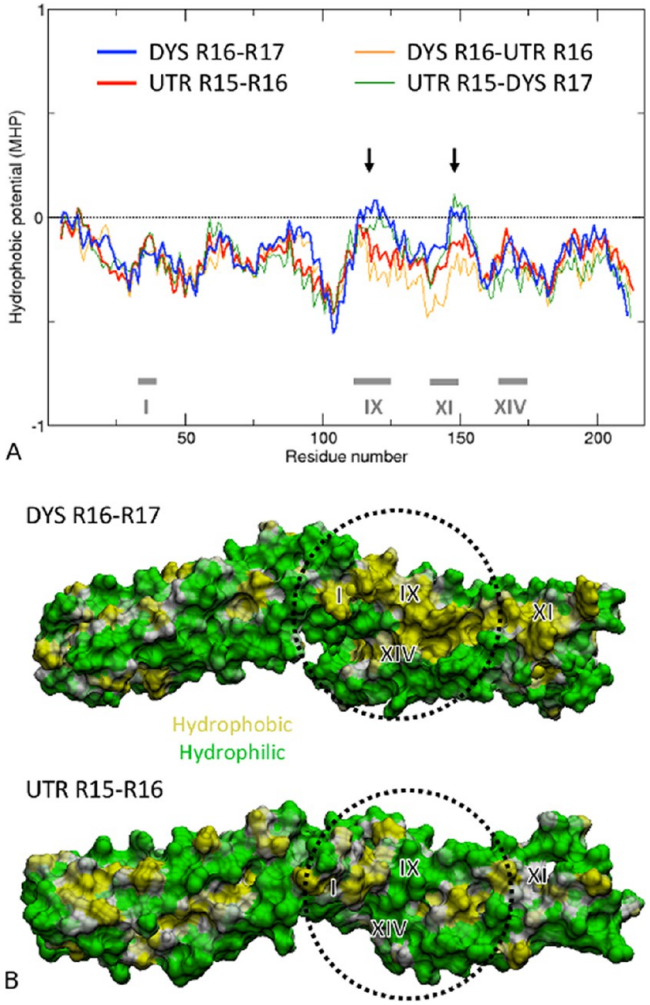

Figure 4. (A) Molecular hydrophobicity potential (MHP) averaged over the major conformational states of the tandem repeats. Arrows indicate the regions showing the major differences between the UTR R15−R16 and DYS R16−R17 fragments. Along the primary sequence, we indicate the position of microdomains I, IX, XI, and XIV that induce the largest modifications of nNOS membrane localization, as reported by Lai and co-workers. (B) 3D representation of the hydrophobic surface potentials of the major conformations of both dystrophin and utrophin tandem repeats as calculated with Platinum. Circles with dashed black lines indicate the region that differentiates between fragments interacting with nNOS and those that do not.

R15−R16 and DYS R16−UTR R16 (Figure 4B and Figure SM3 of the Supporting Information).

Therefore, by comparing the fragments that interact with nNOS to those that do not, we can assume that the dystrophin−nNOS contact region involves the N-terminal part of helix A and the C-terminal part of helix B and/or the N-terminal part of helix C of DYS R17 (Figure 5A). These regions display hydrophobic and neutral molecular surface properties that contrast with the properties of the hydrophilic and acidic surfaces of the homologous utrophin regions. Analysis of the chimeric fragment surface properties confirms these observations.

The hydrophobic residues composing those patches are mostly conserved in the known mammalian and avian dystrophin sequences, but intriguingly, they are also conserved in the utrophin sequences (Figure SM4 of the Supporting Information). Therefore, small primary sequence modulations between dystrophin and utrophin cannot by themselves explain the specificity of interactions with nNOS, and the 3D structural context is thus of primary importance.

3D Organization of the Putative Dystrophin−nNOS Binding Site. The organization of the filamentous structure and the resulting topography of the molecular surface also seem to play roles in the definition of the dystrophin microdomains potentially interacting with nNOS. In the tandem repeats, the organization of the putative nNOS binding site is affected by the proximity of the linker region, the A−B loop of the first coiled-coil repeat, and the B−C loop of the second coiled-coil repeat (Figure 5A). The analysis of the contacts (5.5 Å cutoff) made by the linker region revealed less frequent contacts with the surrounding A−B and B−C loops for the protein fragments that interact with nNOS than for the ones that do not (Figure 5B). This correlates with the global straight or kinked topology of the tandem repeats. In addition, the increase in the number

dx.doi.org/10.1021/bi400794p | *Biochemistry* 2013, 52, 7777−7784

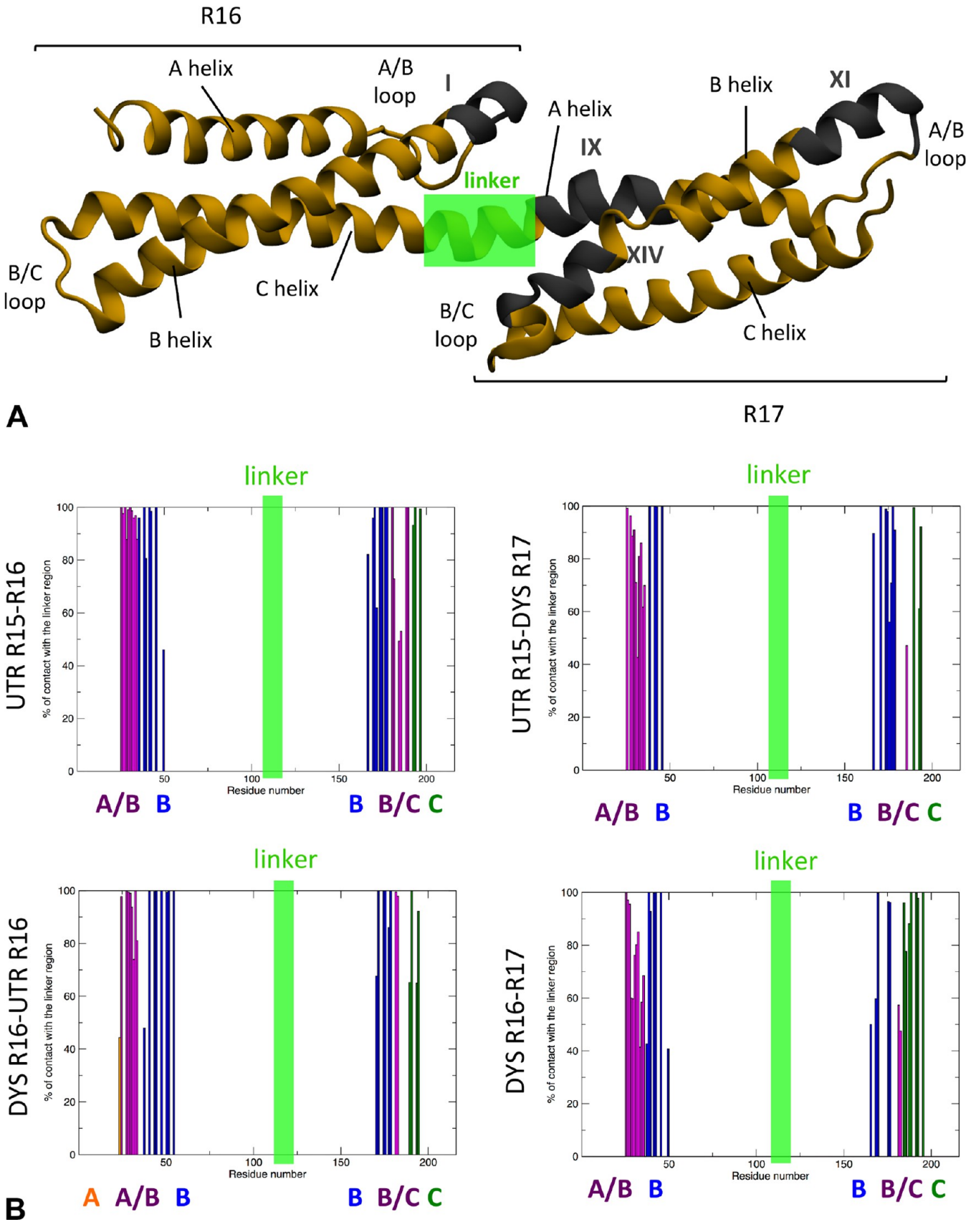

Figure 5. (A) Cartoon representation of the most representative conformer observed during the simulation of DYS R16–R17. Dark gray is used to show the 3D position of the microdomains defined by Lai and co-workers that affect nNOS membrane localization after substitution. (B) Contacts in the vicinity of the linker region for the four tandem repeats. Secondary structure elements are colored orange (helix A), blue (helix B), dark green (helix C), and purple (A–B and B–C loops). The range of the residues chosen to define the linker region is represented by a light green rectangle.

dx.doi.org/10.1021/bi400794p | *Biochemistry* 2013, 52, 7777–7784

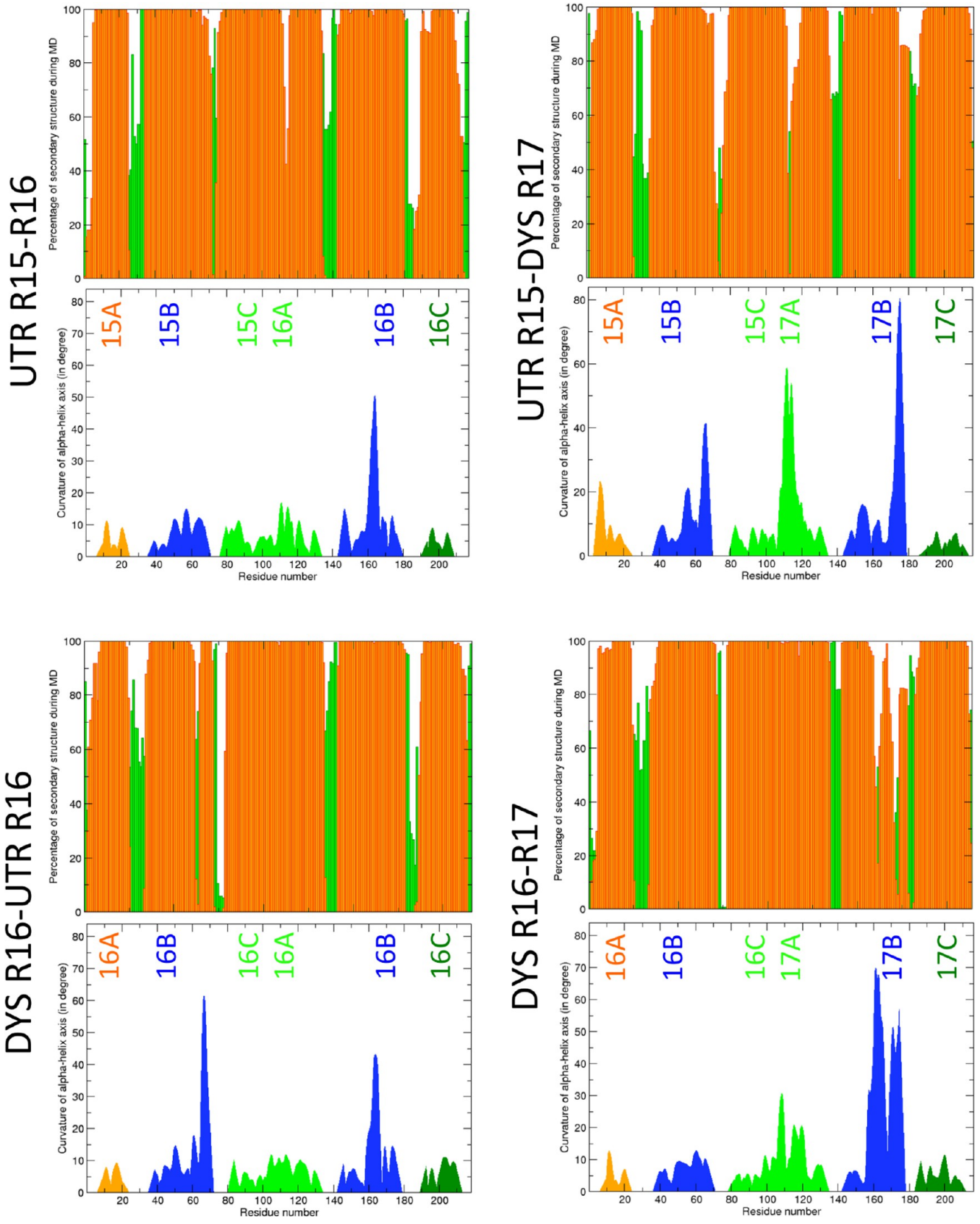

Figure 6. Secondary structure percentage (top) calculated over the four trajectories using Stride. The α-helices and coils are colored orange and green, respectively. Residues belonging to α-helices for >80% of the simulated time define the α-helical coiled-coil structure of the repeats. Kink angle (in degrees, bottom) of the main axis in helical regions, measured using Bendix for the two most representative conformers. Secondary structure elements are colored orange (helix A), blue (both helices B), light green (helix C–A), and dark green (helix C).

dx.doi.org/10.1021/bi400794p | *Biochemistry* 2013, 52, 7777–7784

of R17HC contacts with the linker region, observed for only DYS R16−R17, seems to favor the structuring of the putative nNOS binding site (Figure 5B).

The secondary structure measurements performed on the whole MD trajectories showed that the helices constituting the coiled-coil structure are very stable (Figure 6, top charts). The linker regions of UTR R15−R16 and UTR R15−DYS R17 showed stronger distortions of their helical structure than those of DYS R16−R17 and DYS R16−UTR R16. However, this is not necessarily related to the bending angle of the HCA α-helix (Figure 6, bottom charts). Although a bending at the center of B helices was expected,[13] UTR R15−DYS R17 and DYS R16−R17 presented two new major bending features: (i) the N-terminal extremity of HA located next to the linker region displays a double-inverted bending angle that may expose the putative nNOS binding site, and (ii) a strong bending is observed in the C-terminal part of R17 HB (Figure SM5 of the Supporting Information).

In summary, the putative nNOS-binding site organization depends on three factors: (i) the presence of a neutral and hydrophobic region on R17, adjacent to the linker region, (ii) the kink between two repeats centered on the linker region, and (iii) the bending of α-helices.

DISCUSSION

The dystrophin−nNOS binding region detailed in our analysis is clearly centered on microdomain IX (Arg115−Asn124) of DYS R17, i.e., the same region identified as being essential by Lai and co-workers during their microdomain substitution experiments.[9] However, in our structural models, the spatial proximity of this crucial microdomain IX to microdomain I from DYS R16 (Asp34−Lys40), microdomain XIV (Thr168−Glu175), and the N-terminal part of helix C from DYS R17 allowed us to re-examine their experimental data (Figure 5A). Although this observation was not mentioned by the authors, it appears from the images provided in their study that the microdomain I and XIV substitutions were also accompanied by a partial loss of nNOS membrane localization. Moreover, while the substitution of the DYS R16−R17 linkers by the UTR R15−R16 linker did not modify the nNOS membrane localization, the substitution of entire A or B helices of DYS R16 by DYS R18 resulted in the loss of proper nNOS localization. These results suggest that the A and B helices of DYS R16 are not crucial by themselves for the interaction, but that the A−B loop (only partially covered by microdomain I) is involved in the dystrophin−nNOS interaction. This indicates that changing the residue composition of microdomains I and XIV and/or of the N-terminal extremity of helix C of DYS R17 should modulate the potential surface properties that seem important for strong nNOS binding.

Of interest, the MHP analysis shown in Figure 4 allowed us to highlight a presumed second interaction spot on the R17 repeat of dystrophin. In the vicinity of Tyr148, Trp150, and Tyr151 in microdomain XI, the difference in molecular hydrophobicity potential observed between DYS R17 and UTR R16 could explain the slight modulation in nNOS membrane localization observed with microdomain XI substitution. Substitution of this microdomain could also affect the relative positioning of the A and B helices, destabilizing the crucial hydrophobic patch centered on microdomain IX and thus leading to a decrease in the level of nNOS membrane localization.

The neutral electrostatic nature of dystrophin microdomain IX involved in the interaction with nNOS arises from the balance between the basic (Arg115 and Lys121) and acidic (Asp119) residues of this microdomain. This balance contrasts with the highly acidic (Asp119, Asp121, and Asp122) residues encountered in the homologous region of utrophin. In addition, in the vicinity of this region, a strong hydrophobic patch formed by dystrophin residues Ile122 and Phe123, neither of which is present in utrophin, seems to be crucial for dystrophin−nNOS association.[25]

In addition, the muscles of BMD patients bearing *DMD* gene deletions starting at exon 45 (such as the deletion of exons 45−55[7]) show a decreased level of recruitment of nNOS to the plasma membrane. In these internally deleted dystrophins, the mutation deletes the C-terminal half of R17 and replaces it by the C-terminal part of repeat 22, maintaining only regions I, IX, and XI. As we propose here, this suggests that to maintain the correct 3D platform allowing nNOS interaction, additional regions of R17 are needed. One of these is the N-terminal extremity of helix C of DYS R17, which contributes greatly to the crucial hydrophobic patch centered on microdomain IX.

Building on the remarkable work of Lai and co-workers,[8,9] we are able to conclude that the hydrophobic and neutral molecular surface centered on the N-terminal extremity of helix A and extended by the C-terminal extremity of helix B and the N-terminal extremity of helix C of DYS R17 is the key to dystrophin−nNOS association. The A−B loop of DYS R16 and the B−C loop of DYS R17 may also be essential, as they stabilize this interaction and provide selective surface properties. It should be of great interest to obtain data regarding the nNOS membrane localization after substituting the entire A−B loop of DYS R16 by the loop present in UTR R15. By comparing experimental results to our MD simulations and surface potential calculations, we propose here a precise 3D molecular description of the subdomain of dystrophin that interacts with nNOS. We have provided a complete description of the contribution of essential amino acids to define a new 3D motif for nNOS binding site on dystrophin. Our theoretical structures also offer essential information that could help in the optimization of exon-skipping strategies based on the restoration of the dystrophin−nNOS interaction.[25]

ASSOCIATED CONTENT

Supporting Information

Sequences submitted to the I-TASSER server, I-Tasser *C* scores, and ProCheck analysis, including Ramachandran plots, detailed MD protocols, rmsds of individual repeats calculated over the MD trajectory (Figure S1), electrostatic potentials of DYS R16−UTR R16 and UTR R15−DYS R17 (Figure S2), hydrophobic potentials of DYS R16−UTR R16 and UTR R15−DYS R17 (Figure S3), sequence alignment for the known dystrophin and utrophin homologous repeats in mammalian and avian species (Figure S4), and Bendix study performed for the most populated clusters of DYS R16−R17 (Figure S5). This material is available free of charge via the Internet at http://pubs.acs.org.

AUTHOR INFORMATION

Corresponding Author

*Phone: +33 223 233 007. E-mail: olivier.delalande@univ-rennes1.fr.

Funding

The Association Française contre les Myopathies and Rennes Métropole provided financial support. Computer time was provided by GENCI (IDRIS and CINES, Grant DYSIM 076816).

Notes

The authors declare no competing financial interests.

■ ACKNOWLEDGMENTS

We thank Lai Yi and Donsheng Duan for their work and discussions about their *in vivo* and *in vitro* results for the dystrophin−nNOS interaction.

■ ABBREVIATIONS

BMD, Becker muscular dystrophy; DMD, Duchene muscular dystrophy; DYS, dystrophin; MD, molecular dynamics; MHP, molecular hydrophobicity potential; nNOS, neuronal nitric oxide synthase; rmsd, root-mean-square deviation; rmsf, root-mean-square fluctuation; UTR, utrophin.

■ REFERENCES

(1) Koenig, M., Monaco, A. P., and Kunkel, L. M. (1988) The complete sequence of dystrophin predicts a rod-shaped cytoskeletal protein. *Cell 53*, 219−226.

(2) Koenig, M., Hoffman, E. P., Bertelson, C. J., Monaco, A. P., Feener, C., and Kunkel, L. M. (1987) Complete cloning of the Duchenne muscular dystrophy (DMD) cDNA and preliminary genomic organization of the DMD gene in normal and affected individuals. *Cell 50*, 509−517.

(3) Le Rumeur, E., Winder, S. J., and Hubert, J. F. (2010) Dystrophin: More than just the sum of its parts. *Biochim. Biophys. Acta 1804*, 1713−1722.

(4) Winder, S. J., Gibson, T. J., and Kendrick-Jones, J. (1995) Dystrophin and utrophin: The missing links! *FEBS Lett. 369*, 27−33.

(5) Kusunoki, H., Minasov, G., MacDonald, R., and Mondragon, A. (2004) Independent movement, dimerization and stability of tandem repeats of chicken brain α-spectrin. *J. Mol. Biol. 344*, 495−511.

(6) Deconinck, N., and Dan, B. (2007) Pathophysiology of duchenne muscular dystrophy: Current hypotheses. *Pediatr. Neurol. 36*, 1−7.

(7) Gentil, C., Leturcq, F., Ben Yaou, R., Kaplan, J. C., Laforet, P., Penisson-Besnier, I., Espil-Taris, C., Voit, T., Garcia, L., and Pietri-Rouxel, F. (2012) Variable phenotype of del45−55 Becker patients correlated with nNOSμ mislocalization and RYR1 hypernitrosylation. *Hum. Mol. Genet. 21*, 3449−3460.

(8) Lai, Y., Thomas, G. D., Yue, Y., Yang, H. T., Li, D., Long, C., Judge, L., Bostick, B., Chamberlain, J. S., Terjung, R. L., and Duan, D. (2009) Dystrophins carrying spectrin-like repeats 16 and 17 anchor nNOS to the sarcolemma and enhance exercise performance in a mouse model of muscular dystrophy. *J. Clin. Invest. 119*, 624−635.

(9) Lai, Y., Zhao, J., Yue, Y., and Duan, D. (2012) α2 and α3 helices of dystrophin R16 and R17 frame a microdomain in the α1 helix of dystrophin R17 for neuronal NOS binding. *Proc. Natl. Acad. Sci. U.S.A. 110*, 525−530.

(10) Zhang, Y. (2008) I-TASSER server for protein 3D structure prediction. *BMC Bioinf. 9*, 40.

(11) Zhang, Y. (2009) I-TASSER: Fully automated protein structure prediction in CASP8. *Proteins 77* (Suppl. 9), 100−113.

(12) Roy, A., Kucukural, A., and Zhang, Y. (2010) I-TASSER: A unified platform for automated protein structure and function prediction. *Nat. Protoc. 5*, 725−738.

(13) Legrand, B., Giudice, E., Nicolas, A., Delalande, O., and LeRumeur, E. (2011) Computational study of the human dystrophin repeats: Interaction properties and molecular dynamics. *PLoS One 6*, e23819.

(14) Muthu, M., Richardson, K. A., and Sutherland-Smith, A. J. (2012) The crystal structures of dystrophin and utrophin spectrin repeats: Implications for domain boundaries. *PLoS One 7*, e40066.

(15) Phillips, J. C., Braun, R., Wang, W., Gumbart, J., Tajkhorshid, E., Villa, E., Chipot, C., Skeel, R. D., Kalé, L., and Schulten, K. (2005) Scalable molecular dynamics with NAMD. *J. Comput. Chem. 26*, 1781−1802.

(16) Mackerell, A. D., Jr., Bashford, D., Bellott, M., Dunbrack, R. L., Evanseck, J. D., Field, M. J., Fischer, S., Gao, J., Guo, H., Ha, S., Joseph-McCarthy, D., Kuchnir, L., Kuczera, K., Lau, F. T. K., Mattos, C., Michnick, S., Ngo, T., Nguyen, D. T., Prodhom, B., Reiher, W. E., Roux, B., Schlenkrich, M., Smith, J. C., Stote, R., Straub, J., Watanabe, M., Wiórkiewicz-Kuczera, J., Yin, D., and Karplus, M. (1998) All-atom empirical potential for molecular modeling and dynamics studies of proteins. *J. Phys. Chem. B 102*, 3586−3615.

(17) Mackerell, A. D., Jr., Feig, M., and Brooks, C. L., III (2004) Extending the treatment of backbone energetics in protein force fields: Limitations of gas-phase quantum mechanics in reproducing protein conformational distributions in molecular dynamics simulations. *J. Comput. Chem. 25*, 1400−1415.

(18) Humphrey, W., Dalke, A., and Schulten, K. (1996) VMD: Visual molecular dynamics. *J. Mol. Graphics 14*, 33−38.

(19) Shao, J., Tanner, S. W., Thompson, N., and Cheatham, T. E., III (2007) Clustering molecular dynamics trajectories: I. Characterizing the performance of different clustering algorithms. *J. Chem. Theory Comput. 3*, 2312−2334.

(20) Baker, N. A., Sept, D., Joseph, S., Holst, M. J., and McCammon, J. A. (1998) Electrostatics of nanosystems: Application to microtubules and the ribosome. *Proc. Natl. Acad. Sci. U.S.A. 98*, 10037−10041.

(21) Pyrkov, T. V., Chugunov, A. O., Krylov, N. A., Noldel, D. E., and Efremov, R. G. (2009) Platinum: A web tool for analysis of hydrophobic/hydrophilic organization of biomolecular complexes. *Bioinformatics 25*, 1201−1202.

(22) Frishman, D., and Argos, P. (1995) Knowledge-based protein secondary structure assignment. *Proteins 23*, 566−579.

(23) Dahl, A. C., Chavent, M., and Sansom, M. S. P. (2012) Bendix: Intuitive helix geometry analysis and abstraction. *Bioinformatics 28*, 2193−2194.

(24) Amann, K. J., Guo, A. W., and Ervasti, J. M. (1999) Utrophin lacks the rod domain actin binding activity of dystrophin. *J. Biol. Chem. 274*, 35375−35380.

(25) Harper, S. Q. (2012) Molecular dissection of dystrophin identifies the docking site for nNOS. *Proc. Natl. Acad. Sci. U.S.A. 110*, 387−388.